https://doi.org/10.5194/egusphere-2025-1080
Preprint. Discussion started: 25 March 2025

Three-stage evolution of particle shape in headwater streams

Naoya O. Takahashi[1], Daisuke Ishimura[2], Keitaro Yamada[3], Ryoga J. Ohta[4,5], Yuki Arai[1], Yuki Yamane[1]

[1]Department of Earth Science, Tohoku University, Sendai, 980-0845, Japan
[2]Department of Geography, Tokyo Metropolitan University, Hachioji, Tokyo, 192–0397, Japan
[3]Research Centre for Palaeoclimatology, Ritsumeikan University, Kusatsu, Shiga, 525-8577, Japan
[4]The Institute of Science and Engineering, Chuo University, Tokyo, 112-8551, Japan
[5]Faculty of Humanities, Niigata University, Niigata 950-2181, Japan

Correspondence to: Naoya O. Takahashi (naoya.takahashi.c5@tohoku.ac.jp)

Abstract. Given the importance of sediments in fluvial morphodynamics, studying how sediment particle shapes change during mass loss is important for understanding the morphology and change rates of fluvial landscapes. Particles of riverbed materials tend to become more rounded and circular downstream, but this trend can often be obscured because it results from processes that increase or decrease shape parameters to various degrees. This study unravels such complex interactions by evaluating the contributions of each process and revealing the factors that determine the rates of change in shape. We investigated changes in the roundness and circularity of basalt and shale particles in headwaters using the automated image analysis software Rgrains. The observed evolution of the roundness and circularity comprised three stages with different rates of increase. Both shape parameters initially increased rapidly, remained nearly constant, and then slowly increased downstream, indicating that the dominant process affecting the particle shape changed during a few kilometers of transport. These punctuated shape changes result from the hillslope sediment supply and the addition of rock fragments produced by chipping and fragmentation, of which finer fragments were found to significantly alter the downstream evolution of the shape. The rate of increase in the roundness and circularity of the particle shape depended on the rock type and grain size. The rates for the shale particles were higher than those for the basaltic particles. Grain size clearly affected the shape change rates of basalt particles but not of shale particles. We interpreted these differences between rock type and grain size to be associated with particle durability, weathering mechanisms and speed, and total residence time in the channel. These findings demonstrate that image-based measurements of shape parameters in headwaters enables a detailed examination of the mechanism and rates of changes in particle shape.

https://doi.org/10.5194/egusphere-2025-1080
Preprint. Discussion started: 25 March 2025

1 Introduction

The size and shape of sediment particles dictates their entrainment threshold (Hattingh and Illenberger, 1995; Petit et al., 2015), transport mode (Sklar and Dietrich, 2004; Auel et al., 2017; Demiral et al., 2022), and flux (Vázquez-Tarrío et al., 2019; Cassel et al., 2021; Deal et al., 2023), which ultimately controls the channel hydraulic geometry and erosion rates (Hack, 1957; Sklar and Dietrich, 2004; Parker, 2007). Thus, understanding the evolution of fluvial landscapes requires knowledge of the downstream changes in particle size and shape and mechanisms of particle mass loss. Although many studies have focused on grain size (Paola et al., 1992; Kodama, 1994; Ferguson et al., 1996; Rice and Church, 1998; Attal and Lavé, 2006; 2009; Sklar et al., 2020), studies on shape are also crucial for identifying the causes of grain size changes downstream; this is because changes in size are usually accompanied by changes in shape. In addition, the particle shape reflects the transport history (Wentworth, 1923; Krumbein, 1941a; Benn and Ballantyne, 1994), depositional environment (Brook and Lukas, 2012; Lindsey et al., 2007; Ishimura and Yamada, 2019) and exhumation history (Quick et al., 2020), which enables the distinction of sediments of different origins and reconstruction of sediment provenance.

Among the many parameters to characterize two-dimensional particle shapes (Barrett, 1980; Blott and Pye, 2007), roundness and circularity are the most popular. Roundness is a measure of the corner curvature of a particle (Wentworth, 1919; Wadell, 1932), whereas circularity refers to the similarity of a particle outline to a perfect circle (Cox, 1927). Szabó et al. (2018) used three terms to describe attrition mechanisms under different energy conditions: frictional abrasion, chipping, and fragmentation, which were adopted in this study. Frictional abrasion occurs during rolling and sliding under low-energy conditions and causes flattening of the particle face. Chipping removes a small piece of a particle, particularly from its corners and edges, thereby increasing both roundness and circularity (Domokos et al., 2014; Bodek and Jerolmack, 2021). Fragmentation occurs even under high-energy conditions; cracks formed by particle collisions develop throughout the particle, causing complete breakup of a particle (Bodek and Jerolmack, 2021). These three processes alter particle shape differently.

The dominant attrition mechanism during transport and mass loss rate depend on various factors, such as grain size, transport mode, particle durability, and impact energy during collision (Kuenen, 1956; Zhang and Ghadiri, 2002; Attal and Lavé, 2009; Szabo et al., 2018; Bodek and Jerolmack, 2021; Pfeiffer et al., 2022; Bray et al., 2024). In natural gravel-bed rivers, the bed materials consist of particles with different material properties and transport histories. Although the average roundness and circularity of amalgamated bed material generally increases downstream (Wentworth, 1923; Krumbein, 1941a; Pokhrel et al., 2024), lateral sediment supply from adjacent hillslopes and tributaries can disrupt this trend, as observed for downstream changes in grain size (Rice, 1998; Rice and Church, 1998). Irregular changes in shape parameters owing to lateral sediment supply preclude the estimation of the rates of change in shape parameters with transport distance.

Given the multitude of processes operating in natural rivers, the dominant processes altering the particle shape can change during transport (e.g., Knighton, 1982). This makes the evaluation of the contributions of each process and identification of the causes of changes in particle shape challenging. Although focusing on a short section of a river may help reduce the

https://doi.org/10.5194/egusphere-2025-1080
Preprint. Discussion started: 25 March 2025

number of contributing factors, it requires a very accurate measurement of shape parameters because the absolute changes in roundness and circularity are on the orders of 10^{-2}–10^{-1}. Thus, a study that can link field investigations with laboratory and theoretical studies focusing on the effects of individual processes is required.

One solution is to study the shape evolution of headwaters using image analysis. Both laboratory and field studies have shown that the rate of change in particle shape decreases with the total transport distance or as the particle loses its mass (Wentworth, 1923; Krumbein, 1941a; Domokos et al., 2014; Litwin Miller et al., 2014; Szabo et al., 2018; Bodek and Jerolmack, 2021; Bray et al., 2024). For instance, Bray et al. (2024) investigated the mass loss rates of bulk sediment using a tumbling mill and found that the rates decreased by up to one order of magnitude when the bulk mass was reduced to approximately 90% of its initial value. Thus, headwaters are the best locations for observing significant changes in particle shape over short transport distances.

The advent of image analysis tools has enabled the efficient and reproducible measurement of particle shapes (Roussillon et al., 2009; Zheng and Hryciw, 2015; Cattapan et al., 2024). Image analysis can improve the accuracy of shape measurements by dramatically increasing the number and size of samples. Litwin Miller et al. (2014) conducted manual and image-based measurements of particle shape in headwaters at over 60 sites along a 10 km reach. Despite some scatter in the measured shape parameters, they successfully identified changes in circularity of <0.1 and those in increasing rates of circularity. A large sample size also enables the extraction of information from the distribution of shape parameters. Although the distribution of shape parameters potentially provides insights into the origin of the sediments (Sneed and Fork, 1958; Ishimura and Yamada, 2019), tremendous effort is required to construct smooth histograms, which is impractical when conducting conventional shape measurements (e.g., Krumbein, 1941b; Powers, 1953). Constructing smooth histograms is particularly important for studying the spatial changes in shape distributions. Ishimura and Yamada (2019) measured the roundness of $>10^4$ particles in tsunami deposits by using an image analysis algorithm developed by Zheng and Hryciw (2015). They showed that the sediments of different beaches and rivers can be distinguished using the distribution of roundness. They also revealed the inundation heights of paleotsunamis using the ratio of marine and fluvial sediments estimated from the roundness distributions. Therefore, image-based measurement of the particle shape would benefit the evaluation of the relative contributions of various processes to the downstream changes in the shape parameters.

Motivated by these ideas, we investigated the downstream changes in the roundness and circularity of headwaters using image analysis. We aimed to reveal (1) how various processes interact to cause a downstream increase in roundness and circularity and (2) the effects of rock type and particle size on the rates of change in roundness and circularity. We collected samples of four size classes from the main stream, tributaries, and talus deposits to study the evolution of shape from the beginning of transport. We also performed a manual crushing experiment to estimate the shapes of the particles produced by chipping and fragmentation, which was used to evaluate how these processes affect the distributions of the shape parameters. All samples were separated into two rock types, shale and basalt, and analyzed using the image analysis software Rgrains (Yamada, 2024). We demonstrated that the observed downstream shape changes consisted of three stages with different rates of change. While the spatial pattern was common to both rock types and grain size classes, their rates of change differed. We

https://doi.org/10.5194/egusphere-2025-1080
Preprint. Discussion started: 25 March 2025

evaluated the contributions of the processes that affect the distribution of shape parameters to the observed changes in particle shape and discussed the causes of the three-stage evolution and dependence of the particle shape on the rock type and grain size.

2 Background

2.1 Geologic background

We studied a small river, the Mosawa, located on Tsugaru Mountain in northeastern Japan (Fig. 1). Mosawa is a perennial river and receives 1400 mm y^{-1} of rain on average (Japan Meteorological Agency, 2025). We focused on a 6 km-long reach from the channel head, which drains an area of 4.2 km^2. Miocene basalts and dolerites dominate the upstream part of the studied catchment, and Miocene shale dominates the downstream part (Tsushima and Uemura, 1959; Uemura et al., 1959). The basaltic rocks exposed along streams exhibit various degrees of fracturing and weathering (Tsushima and Uemura, 1959; Uemura et al., 1959). Shale is prone to slaking. The fresh part of the shale is dark gray and turns white when weathered. The exposed bedrock of shale and shale particles found in the bed are mostly white and much more fragile than the basaltic particles. The channel slopes tend to be steeper on basaltic rocks than on shales. The shale reaches have wider banks than the basaltic rocks. A check dam is located in the downstream area (Fig. 1). We observed that coarse grains are mostly trapped in the upstream half of the dammed section, and only fine grains less than several millimeters in diameter are present near the dam wall. Thus, we mainly focused on the reaches upstream of the dam.

Four tributaries with catchment areas >0.1 km^2 supply gravels to the main stream in the studied reach. The catchment area of the most upstream tributary is comparable to that of the main stream at its confluence (Fig. 1). The catchment areas of the other three tributaries are 10–34% of that of the main stream at the confluences. Shale particles are supplied from all four tributaries, whereas basaltic particles are supplied only from two tributaries. These differences in the relative catchment area and lithology suggest that the impact of tributary supply on the evolution of particle shape in the main stream varies among tributaries.

https://doi.org/10.5194/egusphere-2025-1080
Preprint. Discussion started: 25 March 2025

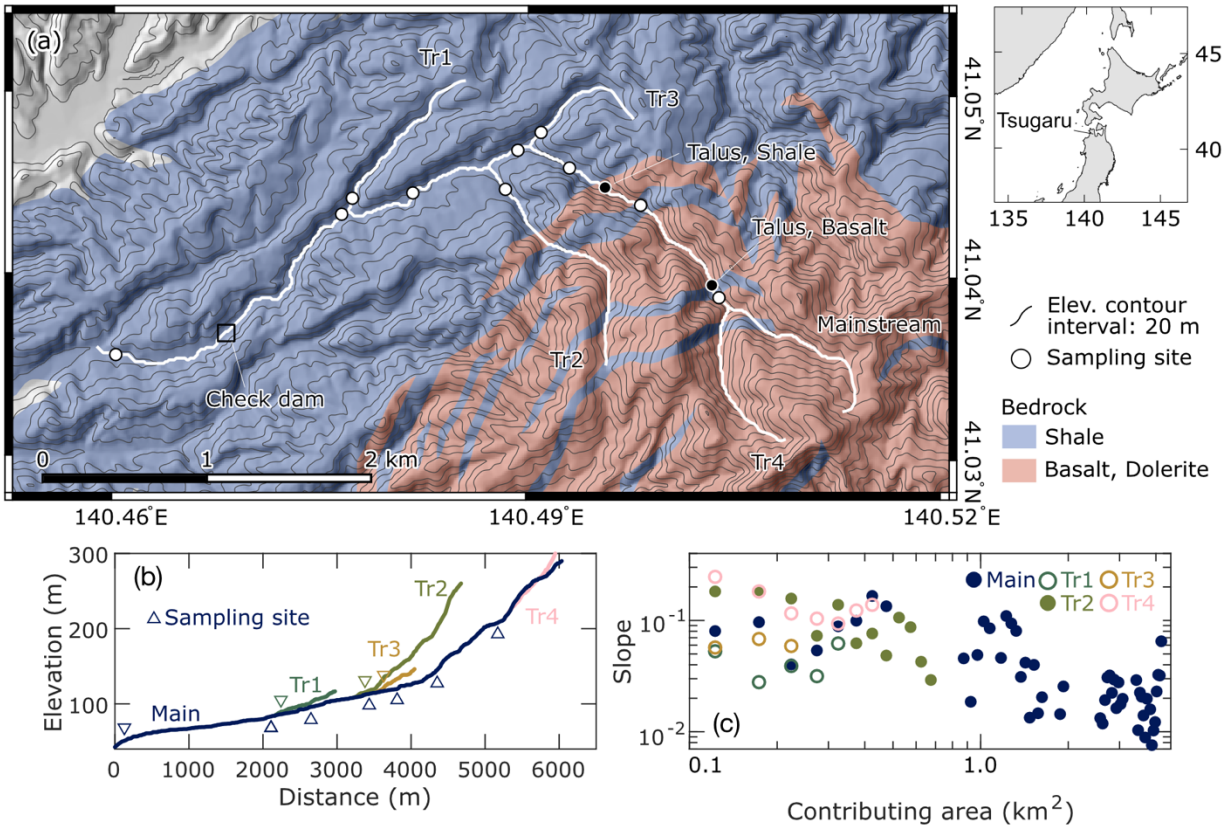

Figure 1: (a) Geologic map of the study area. Geologic units are after Tsushima and Uemura (1959) and Uemura et al. (1959). (b) Longitudinal profiles of the main stream and tributaries (Tr1 to Tr4). Triangles indicate the sampling site locations. (c) A log-log plot of the upstream contributing area and longitudinal channel slope based on a 10 m meshed digital elevation model obtained from the Geospatial Information Authority of Japan. Channel slope is averaged using logarithmic bins.

2.2 Definition of shape parameters and downstream evolution model

In this study, we used the roundness and circularity of the particles. We used Waddell's roundness, a ratio of average radius of curvature of the corners and radius of the maximum inscribed circle (Wadell, 1932). Circularity is the degree to which a two-dimensional outline of a particle is close to that of a circle (Blott and Pye, 2007). Cox (1927) introduced a proxy for roundness, which has also been termed the isoperimetric ratio (IR) in recent studies on particle shapes (Litwin Miller et al., 2014; Quick et al., 2020; Pokhrel et al., 2024)

$$IR = 4\pi AP^{-2}, \quad (1)$$

https://doi.org/10.5194/egusphere-2025-1080
Preprint. Discussion started: 25 March 2025

where A is the projected area of a particle and P is its perimeter. IR represents how close a particle shape is to a circle and is 1 for a perfect circle. Blott and Pye (2007) argued that circularity is a more accurate term for Cox's roundness (IR), because IR is a measure of the overall particle shape rather than individual corners. We follow Blott and Pye (2007) and use IR as a proxy for circularity because roundness and circularity can evolve downstream in different manners (Wentworth, 1923; Russel and Taylor, 1937; Krumbein, 1941a; Pettijohn and Lundahl, 1943; Sneed and Folk, 1958), suggesting that the use of both parameters may provide additional insights into the cause of shape evolution.

Particle roundness and circularity tend to increase nonlinearly with the transported distance (e.g., Wentworth, 1923; Krumbein, 1941a; McPherson, 1971; Mills, 1979; Szabó et al., 2018; Pokhrel et al., 2024). Krumbein (1941a) proposed a formula for the downstream evolution of roundness (R) with transport distance x (km).

$$R = R_{lim} - (R_{lim} - R_0)e^{-\lambda_R x}, \tag{2}$$

where R_{lim} is the limiting roundness, R_0 is the initial roundness before transportation, and λ_R is a coefficient that controls the rate of change in R. The downstream evolution of IR follows the same trend as in Eq. (1) (Krumbein, 1941a).

$$IR = IR_{lim} - (IR_{lim} - IR_0)e^{-\lambda_{IR} x}, \tag{3}$$

where IR_{lim} is the limiting IR, IR_0 is the initial IR before transportation, and λ_{IR} is a coefficient. Assuming R_{lim} and IR_{lim} are 1, Eqs. (2) and (3) can be rearranged as follows:

$$(1 - R)(1 - R_0)^{-1} = e^{-\lambda_R x}, \tag{4}$$

$$(1 - IR)(1 - IR_0)^{-1} = e^{-\lambda_{IR} x}. \tag{5}$$

The left-hand side of these equations is the ratio of the difference between the limiting shape parameters and those at distances x and 0. Changes in λ_R and λ_{IR} were readily observed in semi-log plots (Krumbein, 1941a).

3 Materials and Methods

3.1 Sampling

We collected particles from gravel bars at seven sites in the trunk stream, three sites in the tributaries, and two taluses (Fig. 1). All sampling sites, except for one, were located upstream of the check dam. Talus samples were collected to study the initial distribution of particle shapes when supplied from the hillslopes. We collected particles sized 2–4, 4–8, 8–16, and 16–32 mm using square mesh sieves. For the samples downstream of the check dam, only particles with the finest size range of 2–4 mm were collected. This is because we only found particles of several millimeters immediately downstream of the dam wall, and the rock type composition of the 2–4 mm samples did not change across the dam (basaltic particles constituted 71% and 66–82% of the samples taken downstream and upstream of the dam, respectively). The samples were then dried and separated into shale and basaltic particles based on their color, texture, and hardness. For simplicity, we did not differentiate basalt from dolerite, classifying both as basalts.

https://doi.org/10.5194/egusphere-2025-1080
Preprint. Discussion started: 25 March 2025

3.2 Image analysis

The image analysis procedure involved photographing, pre-processing images, and analyzing particle shapes using Rgrains, an image analysis software (Ishimura and Yamada, 2019; Yamada, 2024) built using an algorithm developed by Zheng and Hryciw (2015). We used MATLAB application v4.11.

Before taking photographs, we aligned the particles with their maximum projected areas parallel to the tray. The tray was placed on a light pad, and a backlit photo was taken from above using a camera mounted on a tripod. Backlit photos are favorable for binarizing the images. Because the results of the image analysis depend on the image resolution, we adjusted the camera height such that the image resolutions for the samples were similar. The resulting image resolutions for the 74 samples ranged between 335 and 348 pix cm^{-1}, with the exception of eight samples with resolutions of 312–319 pix cm^{-1}. We confirmed these differences were unlikely to affect the results, which would be further explained in the next paragraph.

During preprocessing, we first converted the raw images to JPEG images with dimensions of 7358 and 4912 pixels. Results of image analysis depend on the number of pixels per diameter of a circumscribed circle of a particle (PCD: Zheng and Hryciw, 2015). To minimize the dependency of the image analysis on the PCD, we adjusted the PCD values for the 16–32, 8–16, and 2–4 mm particles to those for 4–8 mm particles. Images of 16–32 and 8–16 mm particles were downscaled to 25% and 50% of the original resolutions, respectively, using Adobe Photoshop and Affinity Photo. Images of 2–4 mm particles were upscaled to 200% of the original resolution by bicubic interpolation using a built-in function of Rgrains. After PCD adjustment, particles with a PCD <200 were omitted because their outlines could not be properly identified (Zheng and Hryciw, 2015). Although the particles analyzed using lower-resolution images had slightly lower PCD values than those analyzed using higher-resolution images, such differences were unlikely to affect the results because the values of roundness and circularity did not change with the PCD as long as the PCD exceeded 200 (Zheng and Hryciw, 2015).

The shape parameters were then calculated using the Rgrains. The details of the workflow can be found in Yamada (2024). We first binarized jpeg images using adaptive (Bradley and Roth, 2007) or Otsu (Otsu, 1979) methods and separated the particle and background regions. The extracted particle regions greater than the threshold size were analyzed. The threshold size was adjusted to remove rock fragments that were significantly smaller than the sieve openings. The scales of the images were adjusted according to the original scale of the image and the degree of up- and downscaling. For the other parameters, we used the default settings for Rgrains following the suggestions of Ishimura and Yamada (2019). Rgrains then calculated the Wadell's roundness and *IR* of each particle. We also used other size and shape parameters, namely the radius of curvature of each corner and radius of the maximum inscribed circle. These were recorded in pixels; thus, we converted the unit to millimeters. The number of particles analyzed was greater for smaller particles and basalt. The average number of particles was 3157 and 4938 for the 2–4 mm particles of shale and basalt, respectively, and 253 and 472 for the 16–32 mm particles of shale and basalt, respectively. In total, we analyzed 152932 particles.

https://doi.org/10.5194/egusphere-2025-1080
Preprint. Discussion started: 25 March 2025

To estimate the rates of changes in R and IR (λ_R and λ_{IR}), we fitted Eqs. (2) and (3) to the median R and IR values using the least squares method. We defined the location of the channel head as a point at the valley bottom where 1 m elevation contours bend at an acute angle (Hattanji et al., 2021). The R and IR values of the talus samples were used as the initial R and IR values at the channel head ($x = 0$). Although shale units were not mapped in the most upstream section in the available geological map (distance >5500 m in Fig. 1b), the Wolman count results showed that shale gravel constituted 12–14% of the bed materials in that section (Takahashi, 2025).

To identify the cause of the changes in particle shape, we compared the histograms of R and IR between adjacent sampling sites. The shape of the histogram depends on the choice of bin positions, implying that the calculated changes in relative frequency could be an artifact. To minimize these effects, we used a moving histogram to calculate the changes in relative frequency downstream. We first set the width and the minimum position of the bin to 0.05 and calculated the downstream changes in the relative frequency of a given value of the shape parameters. We then shifted the bin position by one-fiftieth of the bin width and calculated the difference in relative frequency. This process was repeated 49 times. The centers of each bin and their differences in relative frequency were plotted together to form a composite histogram showing downstream changes in particle shape distribution between adjacent sampling sites.

3.3 Manual crushing experiment

To evaluate the impact of chipping and fragmentation on the evolution of particle shape, we conducted a manual crushing experiment. The objectives of this experiment were to reveal the shape distribution of fine rock fragments produced by chipping and fragmentation and the effects of the initial shape distributions on those of the rock fragments. The shape distribution obtained was assumed to be comparable to those produced by natural rivers. This assumption is based on the findings of Domokos et al. (2015) that the distributions of the shape and mass of rock fragments are similar regardless of how the fragments are produced. We used 8–16 mm shale particles taken from the talus and the second-most downstream sites, presumably the least and most rounded and circular samples, respectively. We chose 8–16 mm particles because coarser gravel can produce a greater number of rock fragments, and we could not bring 16–32 mm particles to the laboratory for logistical reasons. When crushing the particles, we smashed the hammer gently and strongly enough to break the particles with a single smash to minimize changes in the particle shape such as flattening of edges. We did not use basalt particles because they are too hard to crush easily. The produced rock fragments were sieved and analyzed in the same manner as the other samples. We focused on rock fragments sized 2–4 mm and compared their shape distributions with those before crushing. We also compared crushed particles with non-crushed 2–4 mm talus particles to determine whether the hillslope sediment supply and production of rock fragments due to chipping and fragmentation had similar impacts on the shape distribution in the main stream.

https://doi.org/10.5194/egusphere-2025-1080
Preprint. Discussion started: 25 March 2025

4 Results

4.1 Shape evolution along the trunk

4.1.1 Roundness

Figures 2a and 2b show the median roundness of the main stream, tributaries, and talus. The shale and basalt talus samples were collected at distances of 4160 and 5150 m, respectively. Their results were plotted at the presumed channel head of 6500 m, assuming that the distributions of roundness in the talus deposit were similar across the catchment.

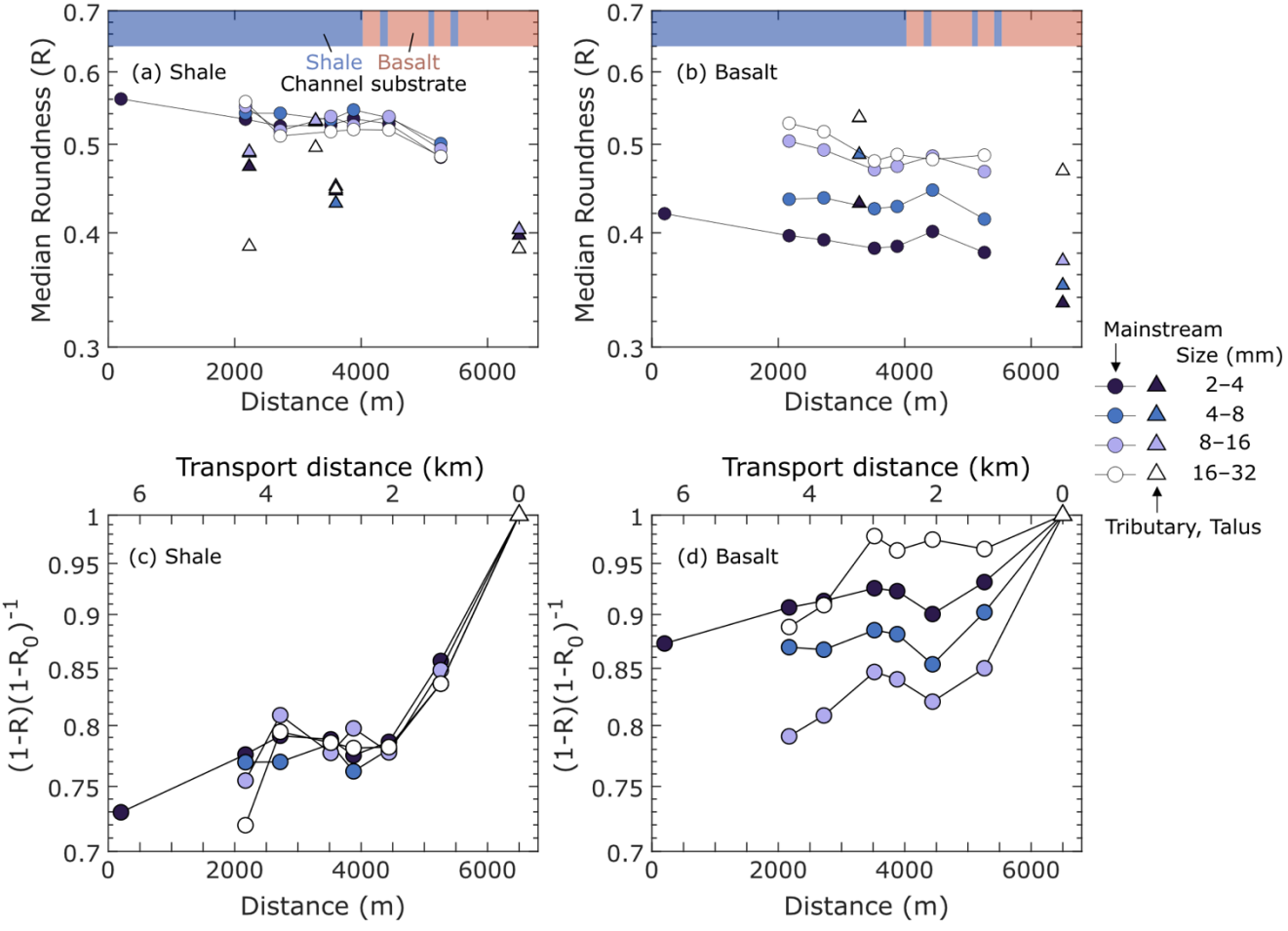

Figure 2: (a, b) Downstream evolution of roundness. (c, d) The ratio of the difference between the limiting roundness and measured roundness at each sampling site (R) and channel head (R_0). Tributary data are plotted at the confluences with the main stream. Talus data are plotted at the presumed channel heads, not at the actual sampling locations. The vertical axis is in a logarithmic scale. In (c, d), the horizontal axis at the top indicates the transport distance (x in Eqs. (4) and (5)) measured from a channel head.

https://doi.org/10.5194/egusphere-2025-1080
Preprint. Discussion started: 25 March 2025

240

The major differences between shale and basalt are that shale particles are more rounded and finer basalt particles have lower *R* values, whereas the *R* of shale particles are similar across the four grain size classes. Except for than these two differences, the downstream evolutions of *R* for shale and basalt particles were essentially similar. The initial roundness of the talus deposits was significantly lower than that of the fluvial samples. Downstream of the channel head, the roundness rapidly
245 increased during the initial 2 km of transport. The median *R* then remained constant or decreased in the middle section between 2720 to 4440 m. In the further downstream section, the median *R* increased. The magnitude of this change was much smaller than that in the most upstream section (>4440 m).

Figure 3 shows the median corner curvature of the particles, inverse of the radius of curvature, and radius of the maximum inscribed circle. Changes in the corner curvature were generally greater than those in the radius of the maximum inscribed
250 circle, indicating that the observed changes in *R* were associated with changes in the corner curvature.

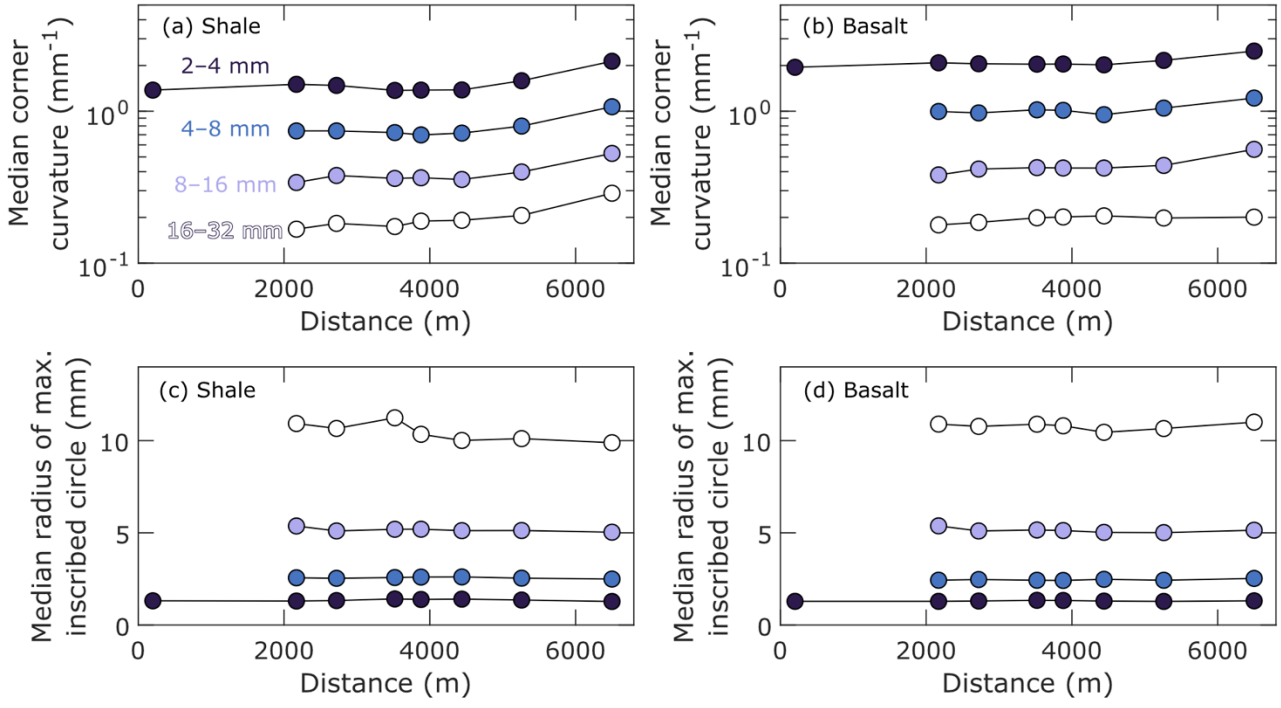

Figure 3: (a, b) Downstream changes in the median curvature of particle corners of shale and basalt, respectively. (c, d) The median radius of the maximum inscribed circle of the shale and basalt particles, respectively.

255

Plotting the left-hand side of Eq. (4) against distance revealed changes in the coefficients (λ_R) within the studied section (Figs. 2c and 2d; Table 1). The rounding coefficient λ_R estimated using all samples in the main stream was larger for shale particles than for basalt (Table 1). The p-values for λ_R were 0.007–0.038, indicating the observed downstream evolution of *R*

https://doi.org/10.5194/egusphere-2025-1080
Preprint. Discussion started: 25 March 2025

is consistent with the general trend (Eq. 2). We also fitted Eq. (2) to data from upstream (distance > 4400 m) and downstream sites (distance < 4400 m). The values of λ_R were much larger in the upstream section than in the downstream section (Table 1). The smaller values of λ_R downstream was partly due to the constant roundness in the middle section. In the upstream section where the *R* values change rapidly, the λ_R values for shale particles did not depend on particle size, whereas those for basaltic particles increased with particle size, except for those sized 16–32 mm (Table 1).

Table 1: Rates of change in roundness.

Extent (distance)	All		>4400 m		< 4400 m	
Grain size (mm)	λ_R (km-1)	p	λ_R (km-1)	p	λ_R (km-1)	p
Shale						
2–4	0.05	0.008	0.12	0.030	0.02	0.070
4–8	0.06	0.017	0.13	0.084	0.00	0.973
8–16	0.06	0.017	0.12	0.037	0.02	0.529
16–32	0.07	0.008	0.12	0.088	0.04	0.330
Basalt						
2–4	0.02	0.007	0.05	0.054	0.02	0.003
4–8	0.03	0.038	0.08	0.035	0.01	0.144
8–16	0.05	0.013	0.10	0.151	0.04	0.042
16–32	0.02	0.017	0.01	0.433	0.06	0.057

Figure 4 shows the changes in the roundness distribution between adjacent sites for 2–4 mm basalt particles. All other histograms of the individual sites and differential histograms were presented by Takahashi et al. (2025). The shapes of these differential histograms differed between the upstream, middle, and downstream sections of the study area.

In the upstream section, where *R* increased rapidly (>4400 m), the differential histogram contained single positive and negative peaks at higher and lower roundness, respectively (Fig. 4a). Figure 4b shows the changes in the roundness distribution when the net decrease in the median *R* is the greatest. When the *R* values were almost constant, the differential histograms often consisted of multiple ridges and troughs (Fig. 4c). The complex shapes of the differential histograms were partly due to the rough shapes of the original histograms. However, these complex changes were found even for 2–4 mm particles, whose minimum sample size exceeded 1000, implying that multiple processes were involved in the observed changes in R.

https://doi.org/10.5194/egusphere-2025-1080
Preprint. Discussion started: 25 March 2025

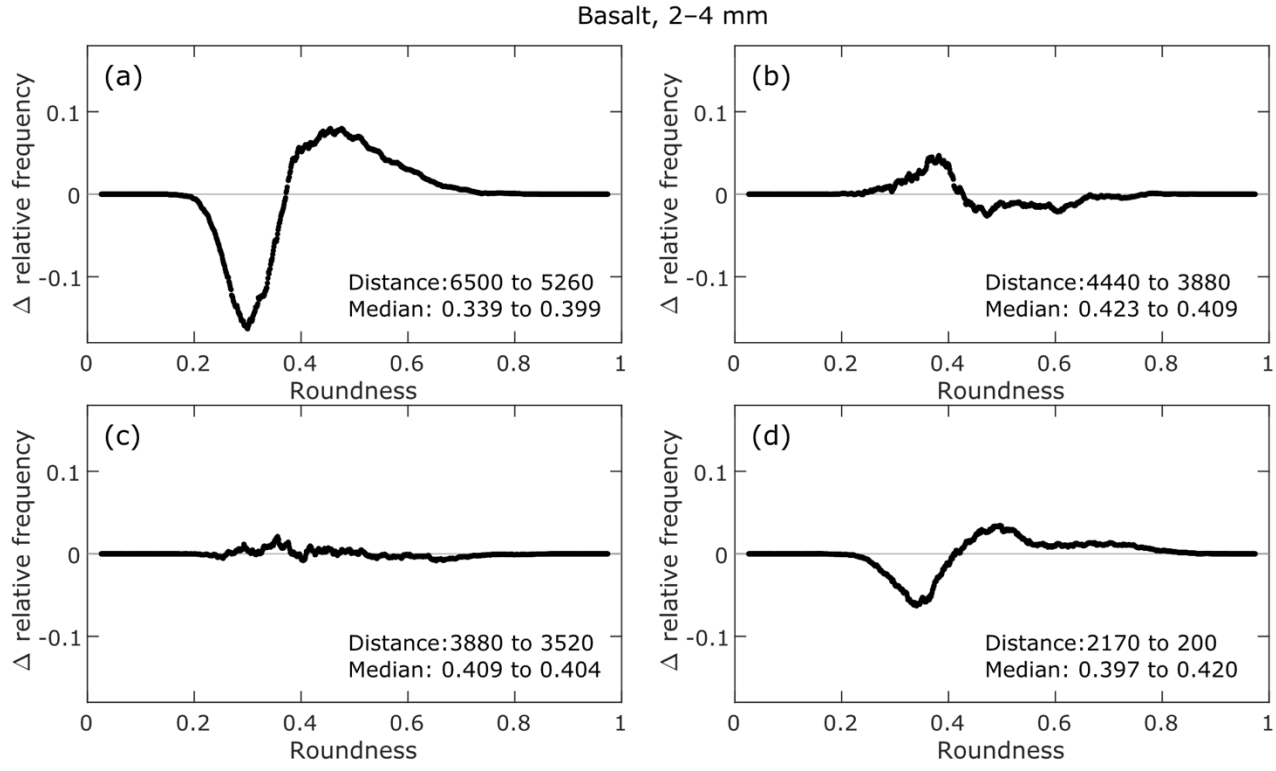

Figure 4: Changes in the roundness (*R*) distribution between adjacent sites. The distance between the two sampling sites and their median *R* values are provided in the lower-right of each panel.

The three tributaries supplied particles with different roundness to the main stream (Fig. 2). The shale particles were less rounded in the three tributaries than in the main stream, potentially contributing to the marginal increase in *R* in the middle part of the study area. However, the changes in the median *R* values were not always consistent with the supply of less-rounded particles from the tributaries. For instance, the transition from initial rapid rounding to punctuated rounding occurs upstream of any tributary junction. In addition, the median *R* values increased significantly between 2170 and 2720 m, where particles with lower *R* were supplied from the tributary to the main stream. These results indicate that tributary supply alone cannot explain the changes in *R* values for shale in the main stream. In contrast, an increase in *R* of the basalt particles occurred concurrently with the supply of rounded particles at the tributary confluence at 3280 m (Fig. 2b). However, the rates of change in *R* across this confluence were not significantly higher than those in the further downstream section, which lacked tributary inputs of basalt particles. Thus, tributary supply alone cannot explain the changes in *R* values for basalt in the main stream.

https://doi.org/10.5194/egusphere-2025-1080
Preprint. Discussion started: 25 March 2025

4.1.2 *IR*

The downstream *IR* evolution was similar to the roundness evolution (Fig. 5). The absolute difference in *IR* between the talus and fluvial samples in the main stream was smaller than that in *R* (Figs. 2 and 5). The *IR* values of both rock types increased rapidly during the first 2 km of transport and stopped increasing thereafter. Unlike roundness, the median *IR* did not evidently increase in the most downstream section, except for 16–32 mm shale particles and 8–16 and 16–32 mm basalt particles.

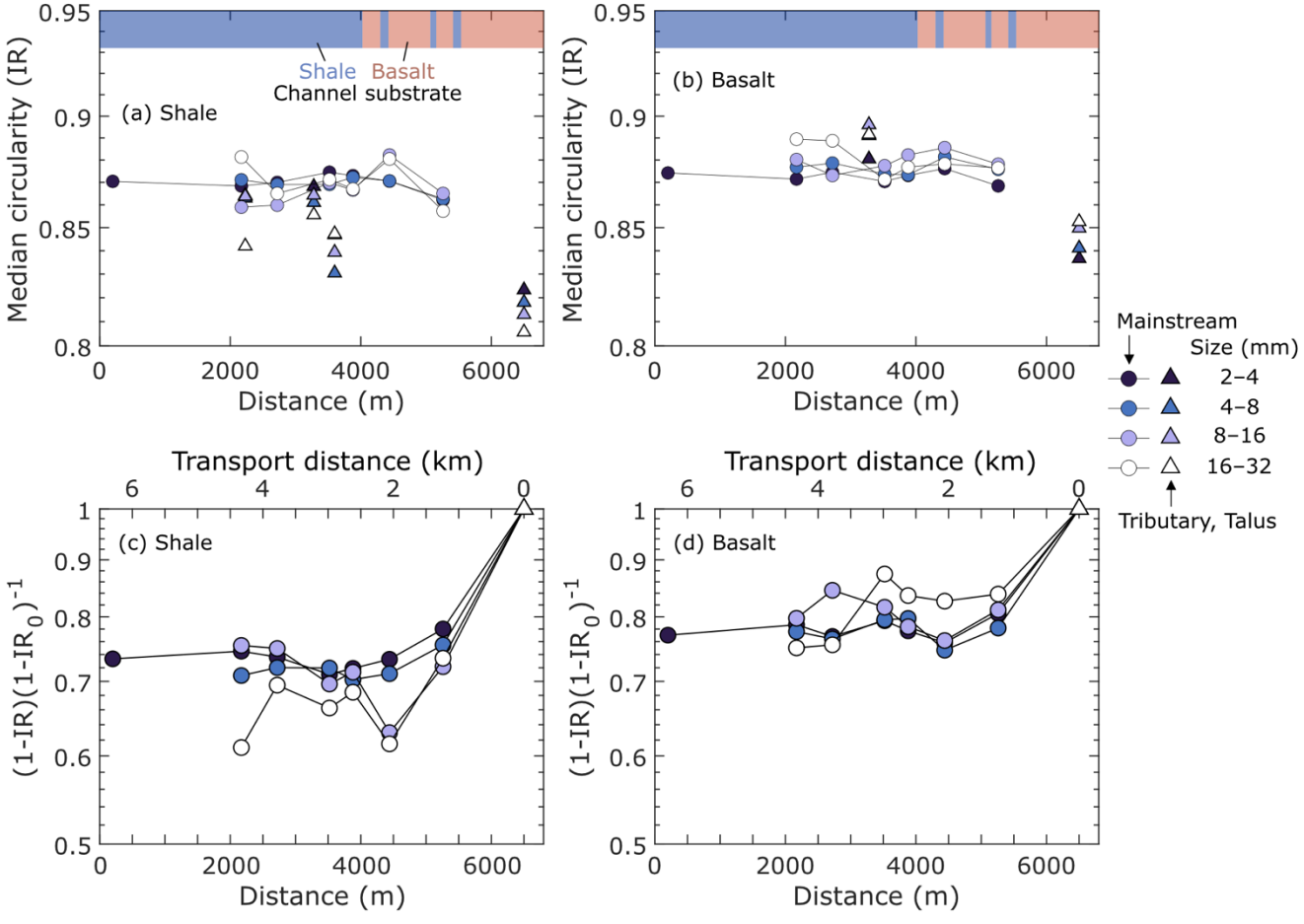

Figure 5: (a, b) Downstream evolution of circularity (*IR*). (c, d) The ratio of the difference between the limiting *IR* and measured *IR* at each sampling site (*IR*) and channel head (IR_0). Tributary data are plotted at the confluences with the main stream. Talus data are plotted at the presumed channel heads, not at the actual sampling locations. The vertical axis is in a logarithmic scale. In (c, d), the horizontal axis at the top indicates transport distance (*x* in Eqs. (4) and (5)) measured from a channel head.

https://doi.org/10.5194/egusphere-2025-1080
Preprint. Discussion started: 25 March 2025

The p-values for the rates of change in *IR* (λ_{IR}) were generally much higher than those for λ_R (Table 2). In the upstream (>4400 m) and downstream (<4400 m) sections, the p-values for λ_{IR} were 0.024–0.215 and 0.126–0.804, respectively.

Table 2: Rates of change in isoperimetric ratio (*IR*)

Extent	All		>4400 m		< 4400 m	
Grain size (mm)	λ_{IR} (km-1)	p	λ_{IR} (km-1)	p	λ_{IR} (km-1)	p
Shale						
2–4	0.05	0.085	0.16	0.137	-0.01	0.306
4–8	0.08	0.037	0.18	0.154	0.00	0.804
8–16	0.06	0.259	0.23	0.073	-0.04	0.127
16–32	0.11	0.034	0.24	0.024	0.04	0.376
Basalt						
2–4	0.04	0.081	0.14	0.125	0.00	0.464
4–8	0.05	0.080	0.15	0.166	0.02	0.186
8–16	0.04	0.168	0.14	0.116	-0.01	0.678
16–32	0.06	0.010	0.10	0.215	0.09	0.126

The differences in *IR* distribution between adjacent sites are presented in Fig. 6 and in Takahashi et al. (2025). Similar to the differential histograms for *R*, the differential histograms for *IR* in the most upstream section were smooth and had single peaks in the positive and negative change domains (Fig. 6a). The histogram shapes in the other sections were much more complex than those in most upstream sections. When the net change in *IR* was small, the histogram was jagged and contained multiple peaks in the positive and negative domains (Fig 6b). When the median *IR* decreased (Fig. 6c), the differential histogram was smoother than when there was little change in the median value *IR* (Fig. 6b).

Particles supplied from tributaries have different *IR* values than those in the main stream. For shale, tributaries fed particles of lower *IR* to the main stream, some of which coincided with a decrease in *IR* in the main stream, such as between 2720 and 3520 m (Fig. 5a). In contrast, although 16–32 mm particles introduced to the main stream at 2230 m had a lower *IR* than those in the main stream, the median *IR* in the main stream significantly increased downstream from the tributary junction (Fig. 5a). For basalt, *IR* values for 16–32 mm particles increased between 2170 and 2720 m, where particles of higher *IR* were supplied from the tributary. However, in the same section, *IR* values for 8–16 mm particles decreased, despite the supply of more circular particles from the tributary.

https://doi.org/10.5194/egusphere-2025-1080
Preprint. Discussion started: 25 March 2025

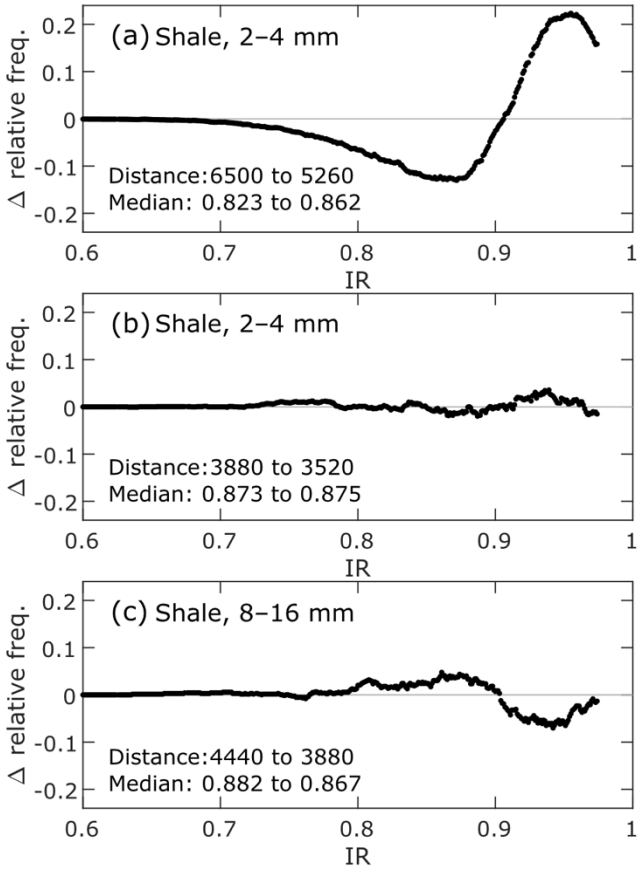

Figure 6: Changes in *IR* distribution between adjacent sites. The distance between the two sampling sites and their median *IR* values are provided in the lower-left of each panel.

4.2 Changes in shape due to manual crushing

The crushed 2–4 mm particles were characterized by lower *R* and *IR* values compared with their original 8–16 mm particles (Fig. 7). The median *R* and *IR* values for the talus samples decreased from 0.403 to 0.390 and 0.813 to 0.797, respectively (Figs. 7a and 7d). The median *R* and *IR* values for the fluvial sample (Loc 6, 2170 m) decreased from 0.550 to 0.393 and 0.859 to 0.795, respectively (Figs. 7b and 7e). Despite the significant differences in the original *R* and *IR* values between the talus and fluvial samples, the distributions of *R* and *IR* values of the crushed particles were almost identical (Figs. 7c and 7f). We also compared the shapes of non-crushed talus samples sized 2–4 mm with the two crushed samples. The distributions of *R* between the non-crushed and crushed particles were similar (Fig. 7c), whereas the distributions of *IR* clearly differed (Fig. 7f).

https://doi.org/10.5194/egusphere-2025-1080
Preprint. Discussion started: 25 March 2025

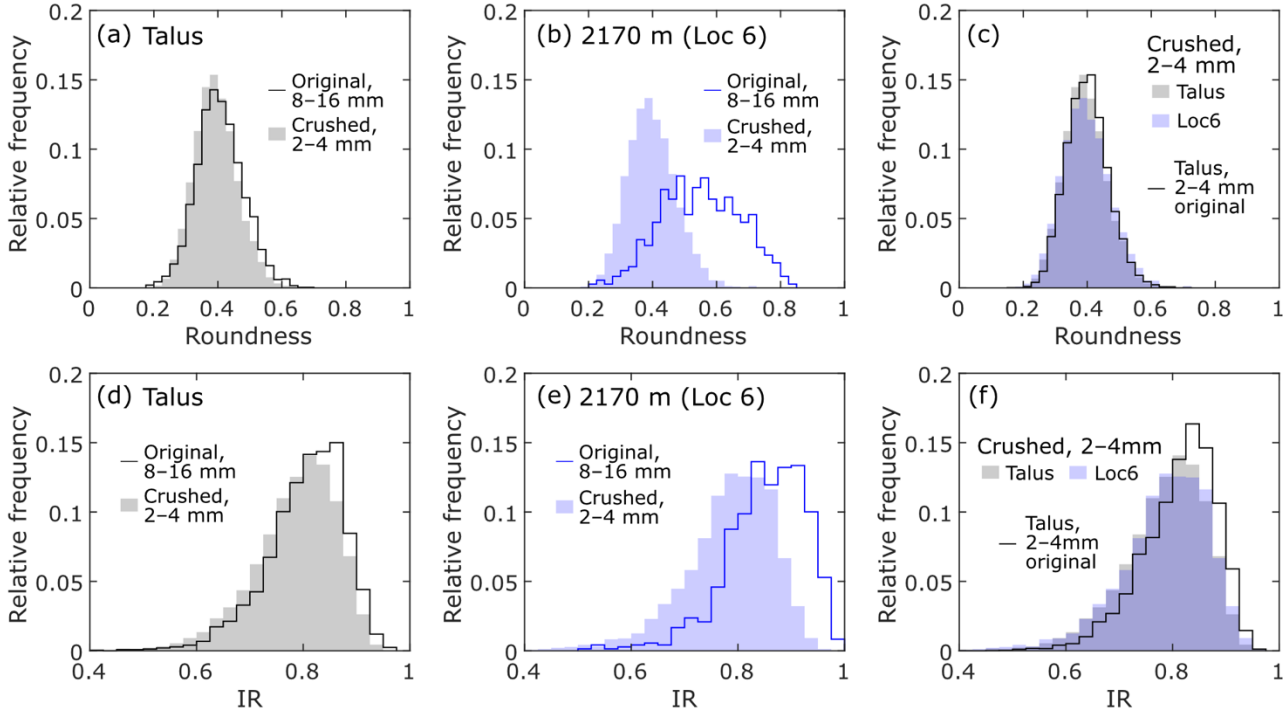

Figure 7: Changes in *R* and *IR* due to manual crushing. Experimental results using (a, d) talus deposits and (b, e) the 6th fluvial sampling point from upstream. (c, f) Comparison between the crushed and non-crushed 2–4 mm talus samples.

To examine the difference in shape parameters between the two crushed 2–4 mm samples and the original talus sample of the same size, we performed a Wilcoxon rank sum test. The sample sizes of the crushed talus, crushed fluvial, and original 2–4 mm talus samples were 11558, 3266, and 6996, respectively, suggesting that the p-values of the test can be very small even if the two samples have almost identical median *R* or *IR* values. To determine whether the p-values changed with sample size, we randomly extracted the specified amount of data from each sample while allowing duplication and performed a Wilcoxon rank sum test. The null hypothesis was that the two samples would have the same median values. The sample size varied from 100 to 50000. For each sample size, we repeated these steps 50 times and obtained 50 p-values for three pairs of samples: crushed talus–crushed fluvial, crushed talus–original talus, and crushed fluvial–original talus. The 16th, 50th, and 84th percentile p-values are presented in Fig. 8. The p-values for *R* significantly exceeded the common threshold value of 0.05 when the sample size was several hundred, and decreased with the sample size (Figs. 8a–8c). This result suggests that the median *R* values of the three samples can be evaluated as different despite the very small difference. For *IR*, the p-values for the crushed talus–crushed fluvial samples were always much higher than 0.05 (Fig. 8d), suggesting that the median *IR* values of the crushed samples were similar, regardless of the initial distribution before crushing. For the

https://doi.org/10.5194/egusphere-2025-1080
Preprint. Discussion started: 25 March 2025

crushed talus–original talus and crushed fluvial–original talus samples, the p-values never exceeded 0.05 (Fig. 8e and 8f), suggesting that the median *IR* values of the crushed samples were differed from that of the talus sample.

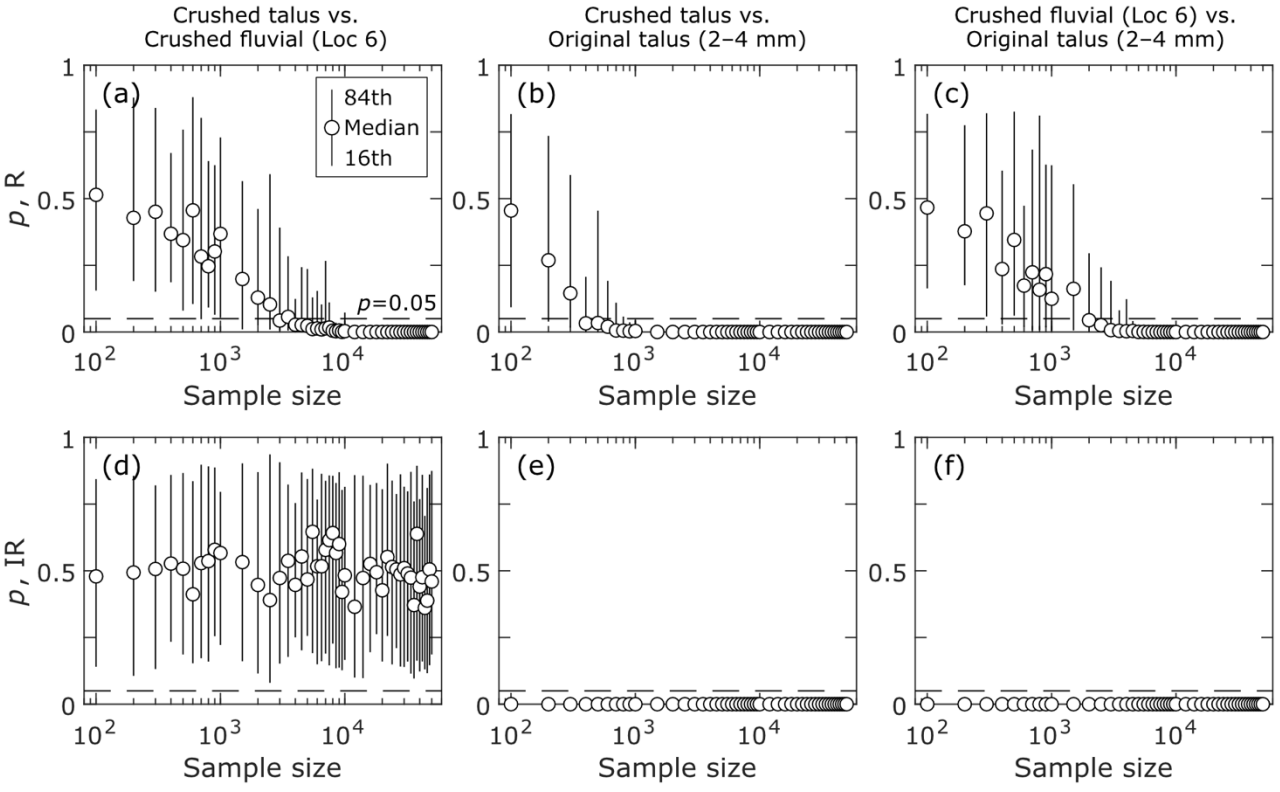

Figure 8: Impacts of sample size on p-values obtained in a Wilcoxon rank sum test. The samples used in the test are (a, d) crushed talus and crushed fluvial samples, (b, e) crushed talus and original 2–4 mm talus samples, and (c, f) crushed fluvial and original 2–4 mm fluvial samples. The dashed line at the bottom of each panel indicates p = 0.05.

5 Discussion

5.1 Downstream shape evolution

The downstream evolution of *R* and *IR* in the studied section comprises three stages with different rates of change. The decrease in λ_R and λ_{IR} with an increase in total transport distance was consistent with the results of other field sites (Wentworth, 1923; Litwin Miller et al., 2014; Szabó et al., 2018; Ishimura and Hiramine, 2025), theoretical models (Domokos et al., 2014; Szabó et al., 2018; Pál et al., 2021), and laboratory experiments (Krumbein, 1941a; Kuenen, 1956; Bodek and Jerolmack, 2021; Litwin Miller and Jerolmack, 2021; Bray et al., 2024). A marginal increase in the shape parameters between rapid and slow increases is less common. Thus, identifying the cause of this punctuated increase can help assess the relative importance of relevant processes and model the downstream evolution of particle shape in nature.

https://doi.org/10.5194/egusphere-2025-1080
Preprint. Discussion started: 25 March 2025

In the most upstream section (>4400 m), R and IR increased much faster than in the rest of the studied section. The transition from initial rapid changes in shape to slower changes occurred 2 km downstream from the channel head, which is consistent with previous findings that a similar transition occurred in the first several kilometers of transport (Wentworth, 1923; Litwin Miller et al., 2014). This rapid change in shape is associated with the removal of sharp corners and edges, which causes a decrease in the curvature of the particle corners (Domokos et al., 2014; Litwin Miller and Jerolmack, 2021). Although obvious, our results confirmed that the rapid increase in R was mostly caused by a decrease in corner curvature rather than by changes in the radius of the maximum inscribed circle (Fig. 3). The differential histograms in the most upstream sections are much simpler than those in the further downstream sections. This result implies that the effect of the rapid removal of sharp corners and edges is much greater than that of other processes, such as the supply from adjacent hillslopes and the production of finer particles with low R and IR values due to chipping and fragmentation.

Following the rapid changes, both shape parameters did not increase in the middle part of the studied section, as shown by much smaller values of λ_R and λ_{IR}. The shapes of the differential histograms are much more complex than those in the most upstream sections. This suggests that multiple processes that increase or decrease R and IR occur in this section. Although the definitions of shape parameters differ among studies, a decrease in shape parameters with transport distance has been reported in fluvial, beach, and aeolian environments (MacCarthy, 1933; Russel and Taylor, 1937; Pettijohn and Lundahl, 1943; Sneed and Folk, 1958; Eisma, 1965; Winkelmolen, 1971; Frostick and Reid, 1980). These studies ascribed the observed decrease to sorting by particle shape or preferential particle breakdown by fragmentation over frictional abrasion. The supply of angular or less circular particles from tributaries and hillslopes can potentially cause local decreases in R and IR. Therefore, identifying the cause of the punctuated increases in R and IR requires a careful examination of the processes that potentially affect the observed shape evolution.

We first considered the effects of the sediment supply from tributaries and hillslopes. The R and IR values in the tributaries were generally different from those in the main stream near the tributary junctions (Figs. 2 and 5). However, changes in the median R and IR values in the main stream did not correspond with those expected from the differences in R and IR between the main stream and tributaries. Moreover, the significant decrease in λ_R and λ_{IR} started upstream of the tributary junctions (Figs. 2 and 5). Thus, we interpreted that the punctuated increases in R and IR were not caused by tributary inputs. For hillslope supply, the sudden decrease in λ_R and λ_{IR} for shale corresponded with the transition of bedrock from basalt to shale at 4000 m (Figs. 2 and 5). Downstream from this bedrock transition, continuous hillslope supply probably contributed to the significant decrease in λ_R and λ_{IR} for shale. The decrease in λ_R and λ_{IR} for basalt occurred at the same location as that for shale. Because basaltic particles are not supplied from the hillslope downstream from the bedrock transition at approximately 4000 m, other processes that counteract an increase in shape parameters are required to explain the observed evolution of the particle shape.

The introduction of grains from coarser to finer size classes owing to mass loss during transport may affect the distribution of R and IR for particles of finer size classes. Although it is unclear whether significant loss of particle mass occurs during a few kilometers of transport, the median grain size estimated from the Wolman pebble count in the studied reach decreased

https://doi.org/10.5194/egusphere-2025-1080
Preprint. Discussion started: 25 March 2025

from 15 to 8.4 cm between 5560 and 1690 m (Takahashi, 2025). In addition, both *R* and *IR* values clearly increased in the studied reach. Thus, the grains that lost their mass and fell into a smaller size class could have affected the observed changes in the particle shape. For shale, *R* and *IR* were similar among the four size classes and did not show systematic changes in grain size (Figs. 2 and 5). For basalt, the coarser grains were more rounded than the smaller grains (Fig. 2). The *IR* values for basalt were similar among the four size classes. These results suggest that the addition of grains from the larger to smaller size classes did not contribute to the punctuated increase in *R* in the middle part.

The production of finer particles from chipping and fragmentation is important in the reduction of λ_R and λ_{IR}. The manual crushing experiment showed that the crushed particles had lower *R* and *IR* values than the parent particles. The experiment also showed that the absolute *R* and *IR* values of the crushed particles were similar regardless of *R* and *IR* values before crushing. The number of rock fragments produced during the particle mass loss can be much larger than that of the parent particles (Litwin Miller and Jerolmack, 2021; Bray et al., 2024). The particle sizes sampled were much smaller than the median grain size of the riverbed materials (Takahashi, 2025), suggesting that the production of finer fragments affected the median *R* and *IR* values.

For shale, coarse particles with lower *R* and *IR* values were continuously supplied from adjacent hillslopes in the middle section. These particles likely produced many fragments during the initial stage of mass loss, lowering λ_R and λ_{IR} in the middle part of the studied reach. Basaltic particles were not supplied to the main stream downstream from the bedrock transition at approximately 4000 m, suggesting that their *R* and *IR* values were less affected by the production of rock fragments than those for shale particles. This interpretation is supported by the fact that the downstream increase in median *R* values for basalt started at 3520 m, whereas that for shale started further downstream (Fig. 2). Nevertheless, basaltic gravels constituted at least 64% of the bed materials in the reaches between 1700 and 5800 m (Takahashi, 2025), suggesting an abundant presence of basaltic grains that can produce fragments. Thus, we argue that the production of finer fragments also contributed to the relatively constant *R* and *IR* of the basalt particles in the middle section of the study area.

The upstream end of the punctuated increase in *R* and *IR* corresponds to a significant decrease in the channel slope, suggesting a change in transport capacity. As in the case of the gravel–sand transition (Dingle et al., 2021), the decrease in transport capacity can change the impact of particle sorting on the composition of bed materials, increasing the proportion of finer and more mobile particles. Previous studies (MacCarthy, 1933; Pettijohn and Lundahl, 1943; Eisma, 1965; Winkelmolen, 1971; Frostick and Reid, 1980) attributed the decrease in roundness or sphericity with transport distance to the effects of shape-sorting because saltating or suspended particles of more irregular shapes can outpace more spherical particles owing to greater drag force (Deal et al., 2023) and smaller settling velocity (Briggs et al., 1962; Dietrich, 1982; Ferguson and Church, 2004). In contrast, when particles roll or slide on a bed, spherical particles tend to travel longer distances than non-spherical particles (Hattingh and Illenberger, 1995; Cassel et al., 2021). Thus, to evaluate whether shape sorting played a role in this study, the dominant transport modes of the sampled particles must be identified.

The finest size range analyzed in the study was 2–4 mm, close to the suspension threshold during typical flood flows in alluvial rivers (Parker et al., 2024). The sizes of the sampled particles were significantly smaller than the median grain size

https://doi.org/10.5194/egusphere-2025-1080
Preprint. Discussion started: 25 March 2025

of the bed material (Takahashi, 2025), suggesting that these finer particles were often sheltered by the surrounding grains. The critical Shields number increases nonlinearly with decreasing grain size relative to the size of surrounding grains (Hodge et al., 2020; Smith et al., 2023). Thus, when the measured fine particles are entrained, their transport stage, which is the ratio of the Shields number to the critical Shields number without the sheltering effect, is likely well above unity.

Considering that the probability of transport by rolling decreases exponentially with the excess transport stage (Auel et al., 2017; Demiral et al., 2022), most of the particles studied were probably saltated or suspended during transport. Therefore, we interpret that the effects of shape sorting partly explained the observed decreases in R and IR. However, this interpretation is admittedly expedient because some studies have shown that the particle shape does not significantly affect the transport distance of saltating particles (Chatanantavet et al., 2013; Demiral et al., 2022). Nevertheless, we argue that the decrease in R and IR in the present study is difficult to explain without the effect of shape sorting because both shale and basalt particles showed a similar decrease at the same location despite their differences in spatial distribution and durability.

In the most-downstream section, where the median R slowly increased, the differential histogram was similar to that of the most-upstream section. Although the absolute difference in R was much smaller than that in the most-upstream section, this result indicates that the combined effects of processes that increase roundness likely prevail over those that decrease roundness. One possible reason for this resurgence of rounding is that the impacts of lateral supply and chipping- and fragmentation-derived rock fragments decrease downstream as the total amount of bed material in the main stream increases. Assuming the number of chipping- and fragmentation-derived fragments decreases as the particle wear proceeds (Bray et al., 2024), the total number of newly added particles per transport distance initially increases downstream and reaches a constant value at some point. In this case, the ratio of new particles to existing grains initially increases and then keeps decreasing. Therefore, without significant sediment supply from tributaries or mass movement, we infer the general rounding process dominate shape evolution of the bed material except for a short river section near a channel head.

Unlike R, IR did not increase downstream (Fig. 5). This is partly because the rock fragments produced by chipping and fragmentation have lower IR values than the talus samples, whereas R values are similar between the rock fragments and the talus samples (Figs. 7 and 8). In addition, while an increase in R requires smoothing of its corners and edges (e.g., Domokos et al., 2014), an increase in IR requires changes in the axis length or overall outline of a particle, suggesting that greater mass loss is required to increase IR than R. Given the relatively slower and smaller changes in IR compared with R, R is more appropriate than IR to study sediment transport or particle mass loss across short distances.

5.2 Factors controlling particle shape

The most evident factor affecting λ_R and λ_{IR} was particle durability (Attal and Lavé, 2009; Bodek and Jerolmack, 2021). Values of λ_R and λ_{IR} were larger for shale than for basalt (Tables 1 and 2). The faster rates of mass loss of the shale particles compared with basalt particles likely resulted from their lower mechanical strength and higher susceptibility to slaking. Most

https://doi.org/10.5194/egusphere-2025-1080
Preprint. Discussion started: 25 March 2025

of the shale particles found in the riverbed were strongly weathered and could be easily crushed manually. In addition, cracks can easily form in the shale particles owing to slaking, making the shale particles susceptible to fragmentation.

The values and changes in R of the basalt particles differed significantly by particle size (Fig. 2). The increase in R with particle size was possibly due to the longer residence time of the coarser particles in the channels (Pettijohn, 1949). In addition, as the particle mass decreases, the effects of viscous damping become increasingly important, hampering the mass loss due to particle collisions (Schmeeckle et al., 2001; Jerolmack and Brzinski 2010). Moreover, the number of finer fragments constitutes greater proportions of the chipping and fragmentation products (Domokos et al., 2015), thereby reducing the median R of finer particles. While we believe these three factors are responsible for the increase in R with particle size, this interpretation may be incompatible with the smallest λ_R for the largest basalt particle (Table 1). We argue that this conflict is related to weathering processes on hillslopes.

The weathering of igneous rocks typically occurs along cooling joints, which eventually produces well-rounded corestones due to spherical weathering (Hirata et al., 2017). However, finer particles produced by weathering detach from coarser particles and experience weathering for a shorter duration, suggesting that they have relatively fresh edges compared with coarser particles. Although rock failures or deep-seated landslides can supply unweathered gravel to channels, large-scale colluvial processes are probably uncommon in the study area because the average angle of hillslopes composed of basalt (distance > 4000 m) was 24.8°, which is smaller than the typical threshold angle above which landslides dominate hillslope denudation (Roering et al., 2007; Larsen and Montgomery, 2012; DiBiase et al., 2023). In addition, our field observations confirmed that most slope failures were shallow and did not supply many boulders to the channels. Therefore, we interpreted that the roundness of the talus deposits of basalt increased with the particle size because of the greater influence of weathering. This resulted in the removal of the angular corners of coarser particles that were otherwise removed at the initial stage of the fluvial transport, leading to a marginal increase in roundness in the headwaters.

While the median R value of basalt clearly depended on particle size, the median IR of basalt did not (Figs. 2 and 5). This is because the maximum IR that a particle can achieve increases with aspect ratio, which is the ratio of the intermediate (b) to the longest (a) axis length (Takashimizu and Iiyoshi, 2016; Quick et al., 2020). The median aspect ratio of the basalt particles decreased with particle size: 0.749, 0.744, 0.739, and 0.731 from the 16–32 to 2–4 mm sized particles. To determine the impact of the aspect ratio on IR, we corrected the effect of the aspect ratio on the measured IR values by diving the IR of the particles by the IR of a perfect ellipse with the same axis ratio IR_t (Villarino, 2005; Quick et al., 2020; Pokhrel et al., 2024). The calculated IR/IR_t values increased with the grain size (Fig. 9), indicating that the insensitivity of IR to the size of the basalt particles was mainly due to the different aspect ratios among the particle sizes. In addition, the downstream change in IR/IR_t was consistent with that of R, confirming the rationale of Quick et al. (2020) that IR/IR_t represents particle roundness.

https://doi.org/10.5194/egusphere-2025-1080
Preprint. Discussion started: 25 March 2025

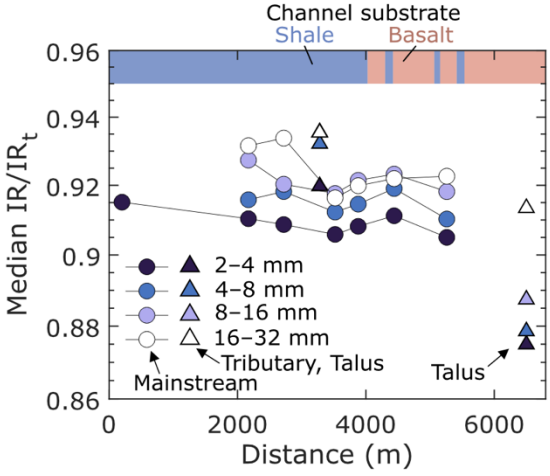

Figure 9: Downstream evolution of IR/IR_t for basalt samples. Tributary data are plotted at the confluences with the main stream. Talus data are plotted at the presumed channel heads, not at the actual sampling locations. The vertical axis is in a logarithmic scale.

The roundness of the shale particles did not clearly change with the grain size (Fig. 2), which is attributed to the rapid weathering of the shale. Sak et al. (2010) investigated the thickness of the weathering rinds of volcanic rocks and found that the rates of weathering rind formation were higher in areas of higher curvature at the rind–core interface. The measured corner curvature of the shale particles increased with decreasing particle size (Fig. 3), indicating that rind formation may be faster for finer particles. Even if the finer and coarser particles have the same rind thickness, as assumed by Jones and Humphrey (1997), the areal or volumetric proportion of the rind within a particle was larger for finer particles, suggesting that weathering has a greater impact on mass loss. Although we did not conduct a chemical analysis of the basalt particles, the lack of a visible weathering rind of basalt particles in the riverbed suggests that such an effect of weathering does not apply to the basalt particles measured in this study.

5.3 Implications for downstream change in particle mass

Although the current analysis enabled the examination of the downstream evolution of particle shape and its rates, it also presents challenges that require further study. First, although we focused on the median R and IR values for simplicity, more information could potentially be obtained from a differential histogram. For instance, basalt particles with R >0.55 clearly increased from 2170 to 200 m (Fig. 4d). The increase in the relative frequency of R was roughly constant between R values of 0.55 and 0.74, which may be incompatible with a general expectation that the rate of increase in R decreases with increasing R (Krumbein, 1941a; Szabó et al., 2018). We speculate that this is related to the supply of well-rounded particles from alluvial storage (Jones and Humphrey, 1997). The shapes of individual histograms, such as the modality, skewness, and kurtosis, may also provide additional insights into the control of flow and material properties on shape evolution. However,

https://doi.org/10.5194/egusphere-2025-1080
Preprint. Discussion started: 25 March 2025

studies under more controlled conditions are required to fully interpret the distribution of shape parameters, because we do not know how various processes operating in natural rivers affect the distribution of shape parameters.

Secondly, we did not consider the effects of particle loss during transport (Sklar et al., 2006; Mueller et al., 2016). If the sediment flux depends on particle shape, fine particles of a certain shape can be preferentially transported over longer distances than other particles and exported out of the catchment, potentially affecting the distribution of shape parameters for finer particles.

Finally, the particles we investigated were much smaller than the median size of the bed materials, suggesting that our findings may not be applicable to studies on particle mass loss in natural rivers that usually focus on median-sized or even coarser grains. The size dependence of the changing rate of shape parameters suggests that inferences on particle mass loss based on particle shape can also differ according to particle size. Although image-based analysis of particle shape has enabled the efficient measurement of riverbed gravel, analyzing the shape of coarse gravel typically found in gravel-bed rivers in steep mountains is still difficult. Given the growing recognition that a coarser fraction of bed material strongly affects the erosion rates and morphology of mountain rivers (MacKenzie et al., 2018; Shobe er al., 2021; Sklar, 2024; Takahashi, 2025), further studies on the size dependency of particle shape evolution are required to link the mass loss of fine particles to the evolution of fluvial landscapes.

6 Conclusion

This study measured the particle shapes of talus deposits and riverbed materials using an automated image analysis tool and examined the downstream changes in particle roundness and circularity and their rates of increase with transport distance. The observed changes in particle shape consisted of three stages with distinct rates of change. The upstream and downstream ends of the study area were characterized by a clear increase in roundness and circularity, with the upstream area showing a much more rapid change. In the intermediate section, roundness and circularity remained almost constant owing to the effects of the hillslope supply and the chipping- and fragmentation-derived finer particles counteracting the increase in both shape parameters. Regarding the effects of rock type and particle size on the changing rates of shape parameters, the rates for shale particles were faster than those for basaltic particles and did not depend on the particle size. In contrast, the rates for coarser basalt particles were higher than those for finer particles. These differences are attributed to the weathering characteristics in the channel and on the hillslopes, the mechanical strength of the particles, and the residence time in the channel. Our findings indicate that because of the significant changes in shape parameters over a short transport distance, headwater streams are suitable for evaluating the contributions of various processes and material properties to downstream changes in shape parameters. Nevertheless, the distribution of shape parameters, rather than a single value, such as a median value, are required to fully use the advantages of image analysis and should be explored in future studies.

https://doi.org/10.5194/egusphere-2025-1080
Preprint. Discussion started: 25 March 2025

Data availability

All particle shape data are available in figshare at http://doi.org/10.6084/m9.figshare.28424138

Author contributions

Conceptualization: NOT. Formal analysis: NOT and DI. Funding acquisition: NOT and DI. Investigation: NOT, DI, RO, YA and YY. Software: KY. Writing – original draft preparation: NOT. Writing – review & editing: All authors.

Competing interests

The authors declare that they have no conflicts of interest.

Acknowledgements

We thank Mikael Attal and Prakash Pokhrel for their helpful discussions. The color maps used in Figs. 2, 3, 5, and 9 were obtained from Crameri (2023). The author would like to thank Editage (www.editage.jp) for English language editing.

Financial support

This research was financially supported by Japan Geographic Data Center and JSPS KAKENHI (Grant Numbers JP21H00631 JP24K00173, and 22KJ2776).

References

Attal, M. and Lavé, J.: Changes of bedload characteristics along the Marsyandi River (central Nepal): Implications for understanding hillslope sediment supply, sediment load evolution along fluvial networks, and denudation in active orogenic belts, in: Tectonics, Climate, and Landscape Evolution, Geological Society of America, https://doi.org/10.1130/2006.2398(09), 2006.

Attal, M. and Lavé, J.: Pebble abrasion during fluvial transport: Experimental results and implications for the evolution of the sediment load along rivers, J. Geophys. Res., 114, 2009JF001328, https://doi.org/10.1029/2009JF001328, 2009.

https://doi.org/10.5194/egusphere-2025-1080
Preprint. Discussion started: 25 March 2025

Auel, C., Albayrak, I., Sumi, T., and Boes, R. M.: Sediment transport in high-speed flows over a fixed bed: 1. Particle dynamics, Earth Surf Processes Landf, 42, 1365–1383, https://doi.org/10.1002/esp.4128, 2017.

Barrett, P. J.: The shape of rock particles, a critical review, Sedimentology, 27, 291–303, https://doi.org/10.1111/j.1365-3091.1980.tb01179.x, 1980.

Benn, D. I. and Ballantyne, C. K.: Reconstructing the transport history of glacigenic sediments: a new approach based on the co-variance of clast form indices, Sedimentary Geology, 91, 215–227, https://doi.org/10.1016/0037-0738(94)90130-9, 1994.

Blott, S. J. and Pye, K.: Particle shape: a review and new methods of characterization and classification, Sedimentology, 55, 31–63, https://doi.org/10.1111/j.1365-3091.2007.00892.x, 2008.

Bodek, S. and Jerolmack, D. J.: Breaking down chipping and fragmentation in sediment transport: the control of material strength, Earth Surf. Dynam., 9, 1531–1543, https://doi.org/10.5194/esurf-9-1531-2021, 2021.

Bradley, D. and Roth, G.: Adaptive Thresholding using the Integral Image, Journal of Graphics Tools, 12, 13–21, https://doi.org/10.1080/2151237X.2007.10129236, 2007.

Bray, E. N., Litwin-Miller, K., Cardona, M., Pettyjohn, S., and Sklar, L. S.: Influence of particle lithology, size and angularity on rates and products of bedload wear: An experimental study, Earth Surf Processes Landf, 49, 4972–4990, https://doi.org/10.1002/esp.6007, 2024.

Briggs, L. I., McCulloch, D. S., and Moser, F.: The hydraulic shape of sand particles, Journal of Sedimentary Research, 32, 645-656, https://doi.org/10.1306/74D70D44-2B21-11D7-8648000102C1865D, 1962.

Brook, M. S. and Lukas, S.: A revised approach to discriminating sediment transport histories in glacigenic sediments in a temperate alpine environment: a case study from Fox Glacier, New Zealand, Earth Surf Processes Landf, 37, 895–900, https://doi.org/10.1002/esp.3250, 2012.

Cassel, M., Lavé, J., Recking, A., Malavoi, J.-R., and Piégay, H.: Bedload transport in rivers, size matters but so does shape, Sci Rep, 11, 508, https://doi.org/10.1038/s41598-020-79930-7, 2021.

https://doi.org/10.5194/egusphere-2025-1080
Preprint. Discussion started: 25 March 2025

Cattapan, A., Gurini, A., Paron, P., Ballio, F., and Franca, M. J.: A method for segmentation of pebble images in the presence of shadows, Earth Surf Processes Landf, 49, 5202–5212, https://doi.org/10.1002/esp.6027, 2024.

Chatanantavet, P., Whipple, K. X., Adams, M. A., and Lamb, M. P.: Experimental study on coarse grain saltation dynamics in bedrock channels, JGR Earth Surface, 118, 1161–1176, https://doi.org/10.1002/jgrf.20053, 2013.

Cox, E. P.: A method of assigning numerical and percentage values to the degree of roundness of sand grains, Journal of Paleontology, 1, 179–183, 1927.

Crameri, F.: Scientific colour maps (8.0.1). Zenodo, https://doi.org/10.5281/zenodo.8409685, 2023.

Deal, E., Venditti, J. G., Benavides, S. J., Bradley, R., Zhang, Q., Kamrin, K., and Perron, J. T.: Grain shape effects in bed load sediment transport, Nature, 613, 298–302, https://doi.org/10.1038/s41586-022-05564-6, 2023.

Demiral, D., Albayrak, I., Turowski, J. M., and Boes, R. M.: Particle saltation trajectories in supercritical open channel flows: Roughness effect, Earth Surf Processes Landf, 47, 3588–3610, https://doi.org/10.1002/esp.5475, 2022.

DiBiase, R. A., Neely, A. B., Whipple, K. X., Heimsath, A. M., and Niemi, N. A.: Hillslope Morphology Drives Variability of Detrital^{10} Be Erosion Rates in Steep Landscapes, Geophysical Research Letters, 50, e2023GL104392, https://doi.org/10.1029/2023GL104392, 2023.

Dietrich, W. E.: Settling velocity of natural particles, Water Resources Research, 18, 1615–1626, https://doi.org/10.1029/WR018i006p01615, 1982.

Dingle, E. H., Kusack, K. M., and Venditti, J. G.: The gravel-sand transition and grain size gap in river bed sediments, Earth-Science Reviews, 222, 103838, https://doi.org/10.1016/j.earscirev.2021.103838, 2021.

Domokos, G., Jerolmack, D. J., Sipos, A. Á., and Török, Á.: How River Rocks Round: Resolving the Shape-Size Paradox, PLoS ONE, 9, e88657, https://doi.org/10.1371/journal.pone.0088657, 2014.

Domokos, G., Kun, F., Sipos, A. Á., and Szabó, T.: Universality of fragment shapes, Sci Rep, 5, 9147, https://doi.org/10.1038/srep09147, 2015.

https://doi.org/10.5194/egusphere-2025-1080
Preprint. Discussion started: 25 March 2025

Eisma, D.: Eolian sorting and roundness of beach and dune sands, Netherlands Journal of Sea Research, 2, 541–555, https://doi.org/10.1016/0077-7579(65)90002-5, 1965.

Ferguson, R. I. and Church, M.: A Simple Universal Equation for Grain Settling Velocity, Journal of Sedimentary Research, 74, 933–937, https://doi.org/10.1306/051204740933, 2004.

Ferguson, R., Hoey, T., Wathen, S., and Werritty, A.: Field evidence for rapid downstream fining of river gravels through selective transport, Geol, 24, 179, https://doi.org/10.1130/0091-7613(1996)024<0179:FEFRDF>2.3.CO;2, 1996.

Frostick, L. E. and Reid, I.: Sorting mechanisms in coarse-grained alluvial sediments: fresh evidence from a basalt plateau gravel, Kenya, JGS, 137, 431–441, https://doi.org/10.1144/gsjgs.137.4.0431, 1980.

Hack, J.T.: Studies of Longitudinal Stream Profiles in Virginia and Maryland. *United States Geological Survey Professional paper*, 294-B, 45–97, https://doi.org/10.3133/pp294B, 1957.

Hattanji, T., Kodama, R., Takahashi, D., Tanaka, Y., Doshida, S., and Furuichi, T.: Migration of channel heads by storm events in two granitic mountain basins, western Japan: Implication for predicting location of landslides, Geomorphology, 393, 107943, https://doi.org/10.1016/j.geomorph.2021.107943, 2021.

Hattingh, J. and Illenberger, W. K.: Shape sorting of flood-transported synthetic clasts in a gravel bed river, Sedimentary Geology, 96, 181–190, https://doi.org/10.1016/0037-0738(94)00139-L, 1995.

Hirata, Y., Chigira, M., and Chen, Y.: Spheroidal weathering of granite porphyry with well-developed columnar joints by oxidation, iron precipitation, and rindlet exfoliation, Earth Surf Processes Landf, 42, 657–669, https://doi.org/10.1002/esp.4008, 2017.

Hodge, R. A., Voepel, H., Leyland, J., Sear, D. A., and Ahmed, S.: X-ray computed tomography reveals that grain protrusion controls critical shear stress for entrainment of fluvial gravels, Geology, 48, 149–153, https://doi.org/10.1130/G46883.1, 2020.

Ishimura, D. and Hiramine, R.: Dispersion, fragmentation, abrasion, and organism attachment of drift pumice from the 2021 Fukutoku-Oka-no-Ba eruption in Japan, Prog Earth Planet Sci, 12, 5, https://doi.org/10.1186/s40645-024-00678-z, 2025.

Ishimura, D. and Yamada, K.: Palaeo-tsunami inundation distances deduced from roundness of gravel particles in tsunami deposits, Sci Rep, 9, 10251, https://doi.org/10.1038/s41598-019-46584-z, 2019.

https://doi.org/10.5194/egusphere-2025-1080
Preprint. Discussion started: 25 March 2025

Japan Meteorological Agency: https://www.jma.go.jp/jma/menu/menureport.html, last access: 30 January 2025.

Jerolmack, D. J. and Brzinski, T. A.: Equivalence of abrupt grain-size transitions in alluvial rivers and eolian sand seas: A hypothesis, Geology, 38, 719–722, https://doi.org/10.1130/G30922.1, 2010.

Jones, L. S. and Humphrey, N. F.: Weathering-controlled abrasion in a coarse-grained, meandering reach of the Rio Grande: Implications for the rock record, Geological Society of America Bulletin, 1997.

Knighton, A. D.: Longitudinal changes in the size and shape of stream bed material: Evidence of variable transport conditions, CATENA, 9, 25–34, https://doi.org/10.1016/S0341-8162(82)80003-9, 1982.

Kodama, Y.: Downstream Changes in the Lithology and Grain Size of Fluvial Gravels, the Watarase River, Japan: Evidence of the Role of Abrasion in Downstream Fining, SEPM JSR, Vol. 64A, https://doi.org/10.1306/D4267D0C-2B26-11D7-8648000102C1865D, 1994.

Krumbein, W. C.: The Effects of Abrasion on the Size, Shape and Roundness of Rock Fragments, The Journal of Geology, 49, 482–520, https://doi.org/10.1086/624985, 1941a.

Krumbein, W. C.: Measurement and Geological Significance of Shape and Roundness of Sedimentary Particles, SEPM JSR, Vol. 11, https://doi.org/10.1306/D42690F3-2B26-11D7-8648000102C1865D, 1941b.

Kuenen, Ph. H.: Experimental Abrasion of Pebbles: 2. Rolling by Current, The Journal of Geology, 64, 336–368, https://doi.org/10.1086/626370, 1956.

Larsen, I. J. and Montgomery, D. R.: Landslide erosion coupled to tectonics and river incision, Nature Geosci, 5, 468–473, https://doi.org/10.1038/ngeo1479, 2012.

Lindsey, D. A., Langer, W. H., and Van Gosen, B. S.: Using pebble lithology and roundness to interpret gravel provenance in piedmont fluvial systems of the Rocky Mountains, USA, Sedimentary Geology, 199, 223–232, https://doi.org/10.1016/j.sedgeo.2007.02.006, 2007.

Litwin-Miller, K., Szabó, T., Jerolmack, D. J., and Domokos, G.: Quantifying the significance of abrasion and selective transport for downstream fluvial grain size evolution, JGR Earth Surface, 119, 2412–2429, https://doi.org/10.1002/2014JF003156, 2014.

https://doi.org/10.5194/egusphere-2025-1080
Preprint. Discussion started: 25 March 2025

Litwin-Miller, K. and Jerolmack, D.: Controls on the rates and products of particle attrition by bed-load collisions, Earth Surf. Dynam., 9, 755–770, https://doi.org/10.5194/esurf-9-755-2021, 2021.

MacCarthy, G. R.: The rounding of beach sands, *American Journal of Science*, *25*(147), 205-224, 1933.

MacKenzie, L. G., Eaton, B. C., and Church, M.: Breaking from the average: Why large grains matter in gravel-bed streams, Earth Surf Processes Landf, 43, 3190–3196, https://doi.org/10.1002/esp.4465, 2018.

McPherson, H. J.: Downstream Changes in Sediment Character in a High Energy Mountain Stream Channel, Arctic and Alpine Research, 3, 65, https://doi.org/10.2307/1550383, 1971.

Mills, H. H.: Downstream Rounding of Pebbles--A Quantitative Review, SEPM JSR, Vol. 49, https://doi.org/10.1306/212F7720-2B24-11D7-8648000102C1865D, 1979.

Mueller, E. R., Smith, M. E., and Pitlick, J.: Lithology-controlled evolution of stream bed sediment and basin-scale sediment yields in adjacent mountain watersheds, Idaho, USA, Earth Surf Processes Landf, 41, 1869–1883, https://doi.org/10.1002/esp.3955, 2016.

Otsu, N.: A Threshold Selection Method from Gray-Level Histograms, IEEE Trans. Syst., Man, Cybern., 9, 62–66, https://doi.org/10.1109/TSMC.1979.4310076, 1979.

Pál, G., Domokos, G., and Kun, F.: Curvature flows, scaling laws and the geometry of attrition under impacts, Sci Rep, 11, 20661, https://doi.org/10.1038/s41598-021-00030-1, 2021.

Paola, C., Parker, G., Seal, R., Sinha, S. K., Southard, J. B., and Wilcock, P. R.: Downstream Fining by Selective Deposition in a Laboratory Flume, Science, 258, 1757–1760, https://doi.org/10.1126/science.258.5089.1757, 1992.

Parker, G., Wilcock, P. R., Paola, C., Dietrich, W. E., and Pitlick, J.: Physical basis for quasi-universal relations describing bankfull hydraulic geometry of single-thread gravel bed rivers, J. Geophys. Res., 112, 2006JF000549, https://doi.org/10.1029/2006JF000549, 2007.

Parker, G., An, C., Lamb, M. P., Garcia, M. H., Dingle, E. H., and Venditti, J. G.: Dimensionless argument: a narrow grain size range near 2 mm plays a special role in river sediment transport and morphodynamics, Earth Surf. Dynam., 12, 367–380, https://doi.org/10.5194/esurf-12-367-2024, 2024.

https://doi.org/10.5194/egusphere-2025-1080
Preprint. Discussion started: 25 March 2025

Petit, F., Houbrechts, G., Peeters, A., Hallot, E., Van Campenhout, J., and Denis, A.-C.: Dimensionless critical shear stress in gravel-bed rivers, Geomorphology, 250, 308–320, https://doi.org/10.1016/j.geomorph.2015.09.008, 2015.

Pettijohn, F. J.: Sedimentary rocks, Harper & Brothers, New York, USA, 526 pp., 1949.

Pettijohn, F. J., and Lundahl, A. C.: Shape and roundness of Lake Erie beach sands. Journal of Sedimentary Research, 13, 69-78, https://doi.org/10.1306/D426919D-2B26-11D7-8648000102C1865D, 1943.

Pfeiffer, A. M., Morey, S., Karlsson, H. M., Fordham, E. M., and Montgomery, D. R.: Survival of the Strong and Dense: Field Evidence for Rapid, Transport-Dependent Bed Material Abrasion of Heterogeneous Source Lithology, JGR Earth Surface, 127, e2021JF006455, https://doi.org/10.1029/2021JF006455, 2022.

Pokhrel, P., Attal, M., Sinclair, H. D., Mudd, S. M., and Naylor, M.: Downstream rounding rate of pebbles in the Himalaya, Earth Surf. Dynam., 12, 515–536, https://doi.org/10.5194/esurf-12-515-2024, 2024.

Powers, M. C.: A New Roundness Scale for Sedimentary Particles, SEPM JSR, Vol. 23, https://doi.org/10.1306/D4269567-2B26-11D7-8648000102C1865D, 1953.

Quick, L., Sinclair, H. D., Attal, M., and Singh, V.: Conglomerate recycling in the Himalayan foreland basin: Implications for grain size and provenance, GSA Bulletin, 132, 1639–1656, https://doi.org/10.1130/B35334.1, 2020.

Rice, S.: Which tributaries disrupt downstream fining along gravel-bed rivers?, Geomorphology, 22, 39–56, https://doi.org/10.1016/S0169-555X(97)00052-4, 1998.

Rice, S. and Church, M.: Grain size along two gravel-bed rivers: statistical variation, spatial pattern and sedimentary links, Earth Surf. Process. Landforms, 23, 345–363, https://doi.org/10.1002/(SICI)1096-9837(199804)23:4<345::AID-ESP850>3.0.CO;2-B, 1998.

Roering, J. J., Perron, J. T., and Kirchner, J. W.: Functional relationships between denudation and hillslope form and relief, Earth and Planetary Science Letters, 264, 245–258, https://doi.org/10.1016/j.epsl.2007.09.035, 2007.

https://doi.org/10.5194/egusphere-2025-1080
Preprint. Discussion started: 25 March 2025

Roussillon, T., Piégay, H., Sivignon, I., Tougne, L., and Lavigne, F.: Automatic computation of pebble roundness using digital imagery and discrete geometry, Computers & Geosciences, 35, 1992–2000, https://doi.org/10.1016/j.cageo.2009.01.013, 2009.

Russell, R. D. and Taylor, R. E.: Roundness and Shape of Mississippi River Sands, The Journal of Geology, 45, 225–267, https://doi.org/10.1086/624526, 1937.

Sak, P. B., Navarre-Sitchler, A. K., Miller, C. E., Daniel, C. C., Gaillardet, J., Buss, H. L., Lebedeva, M. I., and Brantley, S. L.: Controls on rind thickness on basaltic andesite clasts weathering in Guadeloupe, Chemical Geology, 276, 129–143, https://doi.org/10.1016/j.chemgeo.2010.05.002, 2010.

Schmeeckle, M. W., Nelson, J. M., Pitlick, J., and Bennett, J. P.: Interparticle collision of natural sediment grains in water, Water Resources Research, 37, 2377–2391, https://doi.org/10.1029/2001WR000531, 2001.

Shobe, C. M., Turowski, J. M., Nativ, R., Glade, R. C., Bennett, G. L., and Dini, B.: The role of infrequently mobile boulders in modulating landscape evolution and geomorphic hazards, Earth-Science Reviews, 220, 103717, https://doi.org/10.1016/j.earscirev.2021.103717, 2021.

Sklar, L. S.: Grain Size in Landscapes, Annual Review of Earth and Planetary Sciences, 52, 663–692, https://doi.org/10.1146/annurev-earth-052623-075856, 2024.

Sklar, L. S. and Dietrich, W. E.: A mechanistic model for river incision into bedrock by saltating bed load, Water Resources Research, 40, 2003WR002496, https://doi.org/10.1029/2003WR002496, 2004.

Sklar, L. S., Dietrich, W. E., Foufoula-Georgiou, E., Lashermes, B., and Bellugi, D.: Do gravel bed river size distributions record channel network structure?, Water Resources Research, 42, 2006WR005035, https://doi.org/10.1029/2006WR005035, 2006.

Sklar, L. S., Riebe, C. S., Genetti, J., Leclere, S., and Lukens, C. E.: Downvalley fining of hillslope sediment in an alpine catchment: implications for downstream fining of sediment flux in mountain rivers, Earth Surf Processes Landf, 45, 1828–1845, https://doi.org/10.1002/esp.4849, 2020.

Smith, H. E. J., Monsalve, A. D., Turowski, J. M., Rickenmann, D., and Yager, E. M.: Controls of local grain size distribution, bed structure and flow conditions on sediment mobility, Earth Surf Processes Landf, 48, 1990–2004, https://doi.org/10.1002/esp.5599, 2023.

https://doi.org/10.5194/egusphere-2025-1080
Preprint. Discussion started: 25 March 2025

Sneed, E. D. and Folk, R. L.: Pebbles in the Lower Colorado River, Texas a Study in Particle Morphogenesis, The Journal of Geology, 66, 114–150, https://doi.org/10.1086/626490, 1958.

Szabó, T., Sipos, A. Á., Shaw, S., Bertoni, D., Pozzebon, A., Grottoli, E., Sarti, G., Ciavola, P., Domokos, G., and Jerolmack, D. J.: Universal characteristics of particle shape evolution by bed-load chipping, Sci. Adv., 4, eaao4946, https://doi.org/10.1126/sciadv.aao4946, 2018.

Takahashi, N. O.: Relative role of rock erodibility and sediment load in setting channel slope of mountain rivers, Earth Surf Processes Landf, 50, e70017, https://doi.org/10.1002/esp.70017, 2025.

Takahashi, N., Ishimura, D., Yamada, K., Ohta, R., Arai, Y., Yamane, Y.: Shape of natural and manually crushed particles collected from a headwater stream in Tsugaru, Japan, figshare [data set], http://doi.org/10.6084/m9.figshare.28424138, 2025.

Takashimizu, Y. and Iiyoshi, M.: New parameter of roundness R: circularity corrected by aspect ratio, Prog. in Earth and Planet. Sci., 3, 2, https://doi.org/10.1186/s40645-015-0078-x, 2016.

Tsushima, K. and Uemura, F.: Explanatory text of the geological map of Japan, Scale 1:50000, Kodomari. Geological Survey of Japan, 43 pp, 1959.

Uemura, F., Tsushima, K., and Saito, M.: Explanatory text of the geological map of Japan, Scale 1:50000, Kodomari. Geological Survey of Japan, 39 pp, 1959.

Villarino, M. B.: Ramanujan's Perimeter of an Ellipse, https://doi.org/10.48550/arXiv.math/0506384, 20 June 2005.

Wadell, H.: Volume, Shape, and Roundness of Rock Particles, The Journal of Geology, 40, 443–451, https://doi.org/10.1086/623964, 1932.

Wentworth, C. K.: A Laboratory and Field Study of Cobble Abrasion, The Journal of Geology, 27, 507–521, https://doi.org/10.1086/622676, 1919.

Wentworth, C. K.: A field study of the shapes of river pebbles, in: Contributions to the geography of the United States, United States Geological Survey, https://pubs.usgs.gov/publication/b730C, 1923.

Winkelmolen A. M.: Rollability, A Functional Shape Property of Sand Grains, SEPM JSR, Vol. 41, https://doi.org/10.1306/74D72333-2B21-11D7-8648000102C1865D, 1971.

Yamada, K.: Rgarins, GitHub, [software], https://github.com/keitaroyamada/Rgrains, 2024.

Zhang, Z. and Ghadiri, M.: Impact attrition of particulate solids. Part 2: Experimental work, Chemical Engineering Science, 57, 3671–3686, https://doi.org/10.1016/S0009-2509(02)00241-5, 2002.

https://doi.org/10.5194/egusphere-2025-1080
Preprint. Discussion started: 25 March 2025

Zheng, J. and Hryciw, R. D.: Traditional soil particle sphericity, roundness and surface roughness by computational geometry, Géotechnique, 65, 494–506, https://doi.org/10.1680/geot.14.P.192, 2015.